**The mechanism of generating nanoporous Au by de-alloying amorphous alloys**

*

# The mechanism of generating nanoporous Au by de-alloying amorphous alloys

E. M. Paschalidou[1*], F. Celegato[2] , F. Scaglione[1], P. Rizzi[1], L. Battezzati[1]

A. Gebert[3], S. Oswald[3], U. Wolff[3]

L. Mihaylov[4] ,T. Spassov[4]

[1]Dipartimento di Chimica e Centro Interdipartimentale NIS (Nanostructured Surfaces and Interfaces), Università di Torino, Via Pietro Giuria 7, 10125 Torino, Italy

[2]Istituto Nazionale di Ricerca Metrologica (INRIM), Str. delle Cacce, 91, 10135 Torino, Italy

[3]Leibniz- Institut für Festkörper- und Werkstoffforschung (IFW), Helmholtzstraße 20, 01069,Dresden, Germany

[4]University of Sofia "St. Kliment Ohridski", Department of Chemistry and Pharmacy, 1 James Bourchier str., 1164 Sofia, Bulgaria

*Corresponding Author: epaschal@unito.it

## Abstract

De-alloying, i.e. selective dissolution of alloys, is currently studied to produce nanoporous gold items suited for use in catalysis, electrochemical applications, sensors and actuators. Both crystalline and amorphous alloys can be selectively etched. In the former, less noble atoms are removed from surface terraces of grains layer by layer, while noble ones form mounds. These evolve by undercutting and electrolyte percolation to form a ligament network. The mechanism of ligament development by de-alloying amorphous alloys is unknown. Here we show that for de-alloying a Au-based glass, in this case $Au_{40}Cu_{28}Ag_7Pd_5Si_{20}$, percolation of the electrolyte through cracks of the native surface oxide initiates the formation of protuberances which are soon undercut. An interlayer develops, where Au crystals germinate, grow to nanometer size by diffusion and impinge. This is how ligaments start to coarsen. The interlayer is found at all stages between coarsened ligaments and amorphous phase. The ligaments are defective polycrystals, as opposed to single crystals obtained from crystalline alloys.

## 1. Introduction

The selective dissolution of less noble components of an alloy constitutes the process known as de-alloying. The removal of these elements leaves noble atoms on the surface which are deprived of nearest neighbours and diffuse along the solid-electrolyte interface forming clusters. These progressively extend in three dimensions producing a continuous network of ligaments and pores both with size in the nanometer range. The majority of information available to date on the electrochemistry of the de-alloying process and on the resulting structure and morphology of ligaments, derives from experiments performed using either two-component solid solutions, e.g. Ag-Au [1-4], and multicomponent crystalline alloys (e.g. Ag-Au-Pt, Au-Cu-Mn-Zn), or intermetallic compounds having compact structure (e.g. $Al_2Au$) [5-8]. These are polycrystalline alloys having large grains whose structure and size is retained after selective etching. Therefore, each grain becomes a porous single crystal [1,5].

The events occurring during electrochemical de-alloying of crystalline alloys are well described by an operative model of porosity evolution [9-11]. Considering a single alloy grain with nearly flat surface, the stripping of atoms starts from terraces and proceeds layer by layer leaving the more noble Au on the surface as adatoms. These are very mobile and agglomerate rapidly into clusters while further layers are similarly etched so that hillocks grow which passivate the alloy locally trapping some less noble atoms. The distance between hillocks is in the order of a characteristic diffusion length. Then, the electrolyte percolates around these mounds, which are undercut by further de-alloying. The distance between a hillock and a neighbouring one increases to twice the characteristic diffusion length and germination of new clusters occurs. The repetition of this process results in a continuous network of interconnected ligaments and pores [9-11,26].

De-alloying was later performed with materials having complex structure, i.e. intermetallic compounds (e. g. $Al_2Cu$) [23], quasicrystalline phases [24] and multicomponent amorphous alloys [15-20,34]. In these, the removal of the less noble elements and surface diffusion of adatoms induce the formation of numerous new crystals of the stable compact structure of the noble component of the alloy. Since the pristine complex structures of either periodic or amorphous phases are destroyed, germination of the new crystals must occur, contrary to the case of de-alloying crystalline alloys in which the growth of the ligaments takes place epitaxially on the pre-existing phase [5]. The new crystal domains are of nanometers size and seem to grow until their impingement, giving ligaments made of several crystals. To date, detailed observations revealing the mechanism of ligament construction from amorphous alloys are lacking.

Coarsening of microstructures occurs on both prolonged etching and annealing. It has been earlier attributed to diffusive surface smoothening, while later ligament pinch-off due to Rayleigh instability in the solid state was assumed, similarly controlled by surface diffusion [12]. Actually, kinetic studies have shown that coarsening is a thermally activated process with activation energy of the same order as that found in experiments on de-

roughening of gold electrodes due to surface diffusion [13]. At variance, simulations suggested that the coarsening of the interconnected network is due to the collapse of neighbouring ligaments onto each other caused by mechanical stress. After pinch-off at ligament necks, the reduction in surface energy should drive relaxation to the lowest surface energy providing compensation to the plastic work required to bend the ligaments [14]. Experimental evidence of these events is, however, not available.

In this work we employ a good glass forming alloy, $Au_{40}Cu_{28}Ag_7Pd_5Si_{20}$, amorphized by rapid solidification in the form of a ribbon, to reveal aspects of the early stages of the de-alloying process and to unveil the mechanism by which ligaments and pores develop from the amorphous matrix. The alloy has complex composition related to the need for matching glass-forming ability: we have chosen the best glass-forming system based on Au to achieve a fully glassy material by rapid quenching [21]. These features are essential for the understanding of the morphology and microstructure of ligaments as well as of subsequent coarsening events.

## 2. Experimental

A $Au_{40}Cu_{28}Ag_7Pd_5Si_{20}$ master alloy was made by arc melting the pure elements (Au, Ag, Cu, Pd, Si: all 99.99%) in Ar atmosphere. Ribbons were produced by melt spinning: the molten alloy was ejected through the nozzle of a silica crucible onto a Cu wheel rotating at 20 m/s in a chamber evacuated and filled with an Ar partial pressure [18]. The ribbons are 30 μm in thickness on average and 2 mm wide and resulted fully amorphous both in X-ray analyses performed on either side and TEM observations of a thinned sample.

Samples 15 mm in length were cut for use as anode in a PGSTAT302N Potentiostat/ Galvanostat of MetroOhm Instruments in a three electrode cell. 1 M $HNO_3$ aqueous solution was employed for de-alloying at 70°C at the potential of 1.05 V vs Ag/ AgCl using a Pt grid cylinder as a counter electrode. These conditions were previously shown to yield de-alloying with success, producing a continuous and homogeneous nanoporous network [18-20]. A new sample was used as working electrode for every de-alloying experiment. Samples were de-alloyed for 30 s, 1, 3, 5 ,10, 15, and 60 minutes. The critical potential used in this work for de-alloying the Au based amorphous alloy is some mV lower with respect to that used for de-alloying Ag-Au crystalline alloys [2,26], whereas it is higher than that chosen for de-alloying binary Cu-Au crystalline alloys which was anyway far from the transpassive onset potential [25].

Fig. 1 reports anodic polarization curves for the $Au_{40}Cu_{28}Ag_7Pd_5Si_{20}$ amorphous alloy and two crystalline alloys. Both of these were proven by using X-ray Diffraction pattern (XRD) to be constituted by a single fcc phase. The $Au_{37,5}Cu_{47,5}Ag_{6,25}Pd_{8.75,}$ contains the same metal elements as the amorphous alloy although in a different proportion, and the $Au_{31}Cu_{41}Mn_{15.2}Zn_{12.8}$ which was earlier shown to undergo de-alloying with a mechanism typical of crystalline alloys [5]. All curves are complex, although containing some similar

features. The Tafel region is shifted to slightly lower potential in the case of the amorphous alloy, while is very close for the crystalline ones. The transpassive region is very close for the amorphous and the crystalline alloy containing the same elements, whereas it occurs at a potential about 0.2 V lower for the crystalline alloy containing Mn and Zn. In between these potential regions current peaks can be appreciated. As a general behaviour the current density decreases, not surprisingly, in the order $Au_{40}Cu_{28}Ag_7Pd_5Si_{20}$ > $Au_{31}Cu_{41}Mn_{15.2}Zn_{12.8}$ > $Au_{37,5}Cu_{47,5}Ag_{6,25}Pd_{8.75}$. For the amorphous and for $Au_{31}Cu_{41}Mn_{15.2}Zn_{12.8}$ crystalline alloy, the peak potential, is very likely due to the oxidation of Cu, in addition to other less noble elements, e. g. Si as detailed below. The critical potential suitable for de-alloying was found to be just above 1.0 V, since extensive corrosion cracking was experienced by using higher potentials [19]. The $Au_{37,5}Cu_{47,5}Ag_{6,25}Pd_{8.75}$ alloy can be de-alloyed only very slowly as suggested by the low current density and a different electrolyte must be used to obtain a porous network. The reason for the appearance in all curves of a peak in current density at 1.2 V or just above, is not clear yet. Since it appears in all cases, independently of the initial alloy structure or composition, it is supposed that it is due to removal of atoms trapped in Au based crystals, but more work is needed to prove this. The LSV has been performed with a scan rate of 5mV/s.

A Bruker-Atomic Force Microscope Dimension Icon (AFM) was used to examine the sample topography in tapping mode with a scanning of rate 75 Hz. A Si tip on a nitride cantilever (Scanasyst-Air) was employed with a resonance frequency of 78 kHz. The AFM data analysis was made by means of the WSxM5.0 Develop 7.0 software. An Inspect F$^{TM}$ FEG Scanning Electron Microscope (SEM) was also used for checking the morphology of the samples that have been de-alloyed for 30 sec and 1 min in cross section after cutting them under tension load. X-rays Photoelectron spectroscopy (XPS) investigations were performed with a PHI 5600 XPS system using monochromatic Al Kα X-rays (350 W). For profiling samples in the depth, $Ar^+$ ions were used with an energy of 3.5 keV and an angle of around 30 degrees to the surface normal. The sputtering rate was 0.7 nm/min measured with $SiO_2$ reference and the pressure in the XPS analysis chamber was $1*10^{-8}$Pa. Data analysis was made by means of PHI-MULTIPAC software package, V. 9.3, ULVAC-PHI, (1994-2011). A JEOL JEM3010 High-Resolution Transmission Electron Microscope (TEM) was used for the study of the ligaments of a sample de-alloyed afters previous mechanical thinning. A Scanning Transmission Electron Microscope (STEM) was used for the characterization of the ligaments and the porous scaffold after cutting samples using Focussed Ion Beam (FIB).

## 3. Results and Discussion

The surface topography of the as-spun ribbon as revealed using AFM, is made of a grain-like structure (Fig. 2a). The zones displaying uniform contrast are separated by fine cracks having depth in the order of 1 nm. The XPS depth profile of the ribbon (Fig. 2b) reveals an

enrichment in Silicon and Oxygen during the first 6 minutes of sputtering, which corresponds to a depth of about 4 nm. The Si:O ratio suggests the presence of a $SiO_2$ layer on the surface. Therefore, the cracks refer to this layer, apparently formed during the rapid solidification process. It is also noticed that there is a small enrichment of Au on the sub-surface layers of the ribbon. Once these are sputtered away, the elemental concentration becomes that expected from the composition of the alloy. The surface layer appears to influence the etching of the alloy but does not hamper it. In fact, after de-alloying for 30 s, self-similar hilly protuberances appear on the surface (Fig. 3a and b), which reach a height of about 50 nm with respect to the background level. Their lateral extension is between 100 and 200 nm, i. e. that of the silica patches of Fig. 2a. It is inferred that the electrolyte starts penetrating into the alloy through the fine cracks of the oxide layer, initiating the etching at the length scale of these defects. Progressively, removal of atoms extends across the whole surface. Because of the enrichment in Au of the subsurface layer, there might be some atom clusters in crystalline form, which would constitute embryos for the first crystals originated by de-alloying.

While the process continues in the bulk, crystals with random orientation are continuously formed. This might suggest that they are progressively nucleated at the interface with the amorphous matrix, contrary to the case of crystalline alloys in which the original grains do not change structure and provide a substrate for the epitaxial growth of ligaments. However, embryos cannot dissolve back into the amorphous phase once less noble atoms are lost as ions and carried away by the electrolyte, since the process is not reversible. Therefore, this does not appear to be a classical nucleation event. The crystallization is described in a better way as spontaneous germination [22] occurring when Au atoms, freed of nearest neighbours, move to a short distance to self-assemble in their stable close packed structure. The size of the crystalline features observed using TEM for the sample de-alloyed for 30 s (Fig. 4) is compatible with a surface diffusion coefficient in the order of $10^{-19}$ $m^2s^{-1}$, which was earlier determined for the surface movement of Au atoms [18].

The extent of atomic displacement of Au atoms can be inferred by considering the structure of amorphous and liquid Au-Si alloys, which has been determined by X-ray diffraction (XRD) measurements as a function of temperature and simulated by ab-initio molecular dynamics [27-29]. It was shown that it conforms to the model of dense random packing of hard-sphere, with Si atoms coordinating on average 10 Au atoms. Progressive slight densification was found as the temperature decreased down to the eutectic point for the composition $Au_{81}Si_{19}$ [29]. Simulation results showed strong intermixing of the two elements [28]. Should the coordination shell of Si be similarly filled at random by the four metallic atoms of the present alloy, half of them would be less noble than Au and therefore liable to dissolve together with the central Si atom. A subsequent movement at short range of Au atoms, some of which are already nearest neighbours, would enable clustering at multiple locations where fine crystals would form. A different scenario with respect to the initial stage of de-alloying of binary Au-Ag and Au-Cu crystalline alloys where Au atoms cluster epitaxially on the fcc substrate.

To observe the fine structure at this early stage of de-alloying, a sample was mechanically grinded to obtain an electron transparent wedge before de-alloying it for 30 s. It was reckoned that the thinnest zones would reproduce the microstructure of the top layers of a de-alloyed bulk ribbon. The TEM image shown in Fig. 4 reports the result of this experiment. The narrow dark zones contain crystals with a size of a few nanometers, randomly oriented. Their structure is fcc (the diffraction pattern given in the inset of Fig. 4a: rings in the pattern and lattice fringes are compatible with the lattice constant of Au). These zones appear fully de-alloyed, i. e. they were first etched. The mottled contrast of the wider regions in between is due to a mixture of amorphous phase and a large number of Au crystals. The overall microstructure appears to confirm the one displayed in the images of Fig. 3a.

After de-alloying for a longer time (60 s), more atoms are dissolved and the height of the protuberances increases to 85-90 nm while their shape and size is modified. They appear made of bumps, some joined to each other, but none of them exceeding 100 nm in size, i. e. they are definitely smaller than the protuberances found earlier (30 sec). The porosity surrarounding them clearly increased in volume (Fig. 3c and d), showing that there is a preference for atom removal around the base of these features (Fig. 3e and f). This seems to represent a similarity with the de-alloying of crystalline alloys, where the under-cutting of passivated mounds was suggested at the beginning of formation of ligaments rich in Au atoms [10-12].

For a de-alloying time of 3 minutes, the surface is covered by gold particles around 100 nm in diameter, some of which appear knobbly due to coarsening by growth and impingement of crystals on each other (Fig. 5a). After de-alloying for 5 minutes, the increase in size and agglomeration of surface features clearly continues (Fig. 5b), whereas after 10 minutes, the gold hills have transformed into interconnected ligaments with porosity between them (Fig. 5c). The height of these ligaments exceeds 300 nm. There is clear evidence of coarsening by diffusion.

A slice of a sample de-alloyed for 15 min was cut from the ribbon by using FIB and analysed by STEM. Images show the network of ligaments expanding from the external surface into the bulk for about 500 nm (Fig. 6). Their size is uniform and of the same order as those shown in Fig. 5c, indicating that a steady state has been reached in coarsening. In between the ligaments and the pristine amorphous phase, an intermediate wavy layer connecting the amorphous matrix to the ligaments, around 50 nm thick, is well distinguishable (Fig. 6a,c). It is composed of filaments and channels. Observing these zones by TEM, a mixture of the amorphous phase with randomly oriented Au-nanocrystals, as well as a network of Au filaments of the order of 10 nm in size is found (Fig. 6d-e), i.e. the same microstructure as that of the sample mechanically thinned and de-alloyed for 30 s, which was described above. Apparently, this intermediate zone between the amorphous bulk phase and the polycrystalline ligaments demonstrates how the undercutting occurs and how the porosity evolves via percolation of the electrolyte in the newly formed channels.

Comparing this sample with another one that was de-alloyed for 60 minutes (Fig. 6b), the interface between the porous network and the amorphous alloy appears of the same type: about 50 nm thick with a similar de-alloying front. This provides evidence that the same mechanism is operative at all stages of the process. The final size of ligaments depends primarily on the temperature at which the de-alloying is performed and on the type of electrolyte. These parameters can be adjusted to obtain the desired microstructure [18, 19]. The mobility of surface atoms is driven by the reduction in surface energy, therefore, the small pores in the transition zone should play a role in favouring it.

The coarsening of ligaments brings about a typical microstructure as shown in Figs. 5 and in the TEM images of Fig. 7, where the crystals composing the ligaments display grooves on the external surface. Internally, they contain stacking faults or twin boundaries. The latter feature is indicative of a microstructure resulting from grain impingement. Actually, in a different context of encounters of nanoparticles floating in a liquid medium, which gave rise to microstructures analogous to the present ones, the attachment between some of them occurred at a favourable orientation, with faults accounting for the mismatch in lattice stacking [30]. Models of coarsening after de-alloying crystalline alloys have appeared in the literature, suggesting ligament pinch-off due to Raleigh instability, which would determine the topology of the ligament network [12,26]. At variance, a mechanically driven pinch-off and collapse of neighbouring ligaments onto each other has been proposed, taking into account the local stresses due to atom removal [14]. Our microscopy observations of de-alloyed amorphous alloy did not provide evidence in this context, but revealed the occurrence of an intermediate layer between the amorphous matrix and grown ligaments, in which the processes of germination and impingement takes place.

The fully de-alloyed ribbon was found to have undergone contraction of up to 30% in the thickness direction, whereas the width did not change appreciably. This is not surprising, since the ribbon is a few tens of microns thick, therefore the lateral contraction is negligible in comparison to its width. The amorphous backbone of the structure is present until the end of the process and must impose a shear stress on the intermediate layer. Since there is no direct evidence of ligaments breaking, it is concluded that the stress is distributed across the whole intermediate layer and that the loss of volume occurs in the growth direction. This is a feature specific of amorphous alloys, which was never reported for the de-alloying of crystalline ones. A general finding related to this discussion is that a glassy ribbon de-alloyed from both sides, is easily separated into two layers [20] by a fracture surface in its middle. This is located where the very last portion was etched and the two interlayers met. The occurrence of shrinkage on de-alloying has been shown earlier in both crystalline binary alloys [31] and amorphous thin films [32]. Our findings show the relevance of the interlayer in the case of amorphous ribbons, which progressively moves during the process, accommodating the intervening stresses.

The permanence of surface grooves even after prolonged etching is also a specific feature found in de-alloying of amorphous metals. This appears due to the extensive surface diffusion during coarsening. The formation of grooves at triple points between a grain

boundary and external grain surfaces was classically described as a surface diffusion phenomenon, which was driven by the decrease in free energy caused by the movement of atoms away from the grain boundary [33]. Grooves form when local thermodynamic equilibrium between the boundary and the intersected external surface is established. Since it is known that some less noble atoms remain trapped in the ligaments after de-alloying (Supplementary figures and text) [36], it is deduced that these could be segregated to defects in case the partitioning is thermodynamically favoured. This can help in enhancing the chemical activity of the porous material, which was shown to be active in catalysing the oxidation of methanol [17,20] and in enhancing the Raman response of adsorbed molecules [35].

## 4. Conclusions

In this work, the de-alloying mechanism during electrochemical etching of an amorphous Au-based alloy has been studied in detail by means of various microscopy observations: from the very early moments of etching up to the extensive development of a porous network.

The potential range at which the majority elements are removed was reported in order to fix the de-alloying potential at 1.05 V. A native layer of Si oxide was found on the surface of the $Au_{40}Cu_{28}Ag_7Pd_5Si_{20}$ alloy, which was chosen for the experiments. The electrolyte penetrates through the cracks of the layer in a few seconds, forming channels and leaving protuberances of size in the order of a few hundred nanometers. These are then excavated laterally and in depth to give isolated fine crystals at first and then ligaments by impingement of the growing crystals.

The key feature shown in the early stages and in the subsequent movement of the front between the porous layer and the matrix, is the occurrence of an interlayer about 50 nm in thickness formed by filaments around 10 nm wide, voids, as well as residues of the amorphous phase embedded with Au nanocrystals.

Ligaments emerge from the interlayer after an appropriate de-alloying time. They coarsen in a few minutes to a size dependent on the temperature at which the process is performed and do not change appreciably during the progress of the de-alloying. The ligaments are made of adjoined fine crystals containing planar lattice defects. It is deduced that the nanocrystals formed at the interface with the amorphous phase grow by addition of Au atoms and impinge on each other, giving rise to a three dimensional scaffold. During these steps, pores develop in between ligaments. In spite of the occurrence of these voids, a substantial portion (up to 30%) of the original volume of the material is lost. It is speculated that the interlayer sustains the stress due to shrinkage in the direction normal to that of growth.

The coarsened ligaments display grooves on the surface, apparently due to equilibrated grain boundaries.

**Acknowledgements**

This work was supported by the funding scheme of the European Commission, Marie Curie Actions — Initial Training Networks (ITN) in the frame of the project VitriMetTech — Vitrified Metals Technologies and Applications in Devices and Chemistry, 607080 FP7-PEOPLE-2013-ITN and of the project 286205 – BeyondEverest, FP7-REGPOT-2011-1.

**References**

[1]. J. Weissmüller, R. Newman, H. Jin, A. Hodge, J. Kysar Nanoporous metals by alloy corrosion: Formation and mechanical properties., *Mater. Res. Soc. Bull*. 34 (2009) 577–586.

[2]. J. Erlebacher, R. Seshadri, Hard materials with tunable porosity. *MRS Bulletin* 34 (2009) 561–568.

[3]. Z. Qi, J. Weissmuller, Hierarchical Nested-Network Nanostructure by De-alloying. *ACS Nano* 7 (2013) 5948–5954.

[4]. T. Fujita, P. Guan, K. McKenna, X. Lang, A. Hirata, L. Zhang, T. Tokunaga, S. Arai, Y. Yamamoto, N. Tanaka, Y. Ishikawa, N. Asao, Y. Yamamoto, J. Erlebacher, M. Chen, Atomic origins of the high catalytic activity of nanoporous gold. *Nat. Mater*. 11 (2012) 775-780.

[5]. F. Scaglione, F. Celegato, P. Rizzi, L. Battezzati, A comparison of de-alloying crystalline and amorphous multicomponent Au alloys. *Intermetallics* 66 (2015) 82-87.

[6]. A. V. Adrián, R. C. Newman, Nanoporous Metals Fabricated through Electrochemical Dealloying of Ag-Au-Pt with Systematic Variation of Au:Pt Ratio. *J. Electrochem*. Soc. 161 (2014) C1-C10.

[7]. M. B. Vukmirovic, N. Dimitrov, K. Sieradzki, De-alloying and corrosion of Al alloy 2024-T3. *J. Electrochem*. Soc. B 149 (2002) 428–439.

[8]. Z. Zhang, Y. Wang, Z. Qi, C. Somsen, X. Wang, C. Zhao, Fabrication and characterization of nanoporous gold composites through chemical dealloying of two phase Al–Au alloys. *J. Mater. Chem*. 19 (2009) 6042-6050.

[9]. J. Erlebacher, M. J. Aziz, A. Karma, N. Dimitrov, K. Sieradzki, Evolution of nanoporosity in de-alloying. *Nature*. 410 (2001) 450-453.

[10]. J. Erlebacher, at al. An atomistic description of dealloying. *J. Electrochem. Soc*. 151 (2004) C614–C626.

[11]. J. Rugolo, J. Erlebacher, K. Sieradszki, Length scales in alloy dissolution and measurement of absolute interfacial free energy. *Nat. Mater* 5 (2006) 946-949.

[12]. J. Erlebacher at al. Mechanism of Coarsening and Bubble Formation in High-Genus Nanoporous Metals. *Phys. Rev. Lett*. 106 (2011) 225504.

[13]. G. Andreasen, M. Nazzarro, J. Ramirez, R. C. Salvarezza, A. J. Arvia, Kinetics of Particle Coarsening at Gold Electrode/Electrolyte Solution Interfaces Followed by *In Situ* Scanning Tunneling Microscopy, *J. Electrochem. Soc.* 143 (1996) 466–471.

[14]. K. Kolluri et al. Coarsening by network restructuring in model nanoporous gold. *Acta Mater*. 59 (2011) 7645.

[15]. J. Yu, T. Sakurai, Y. Ding, C. Xu, M. Chen, A. Inoue, Nanoporous Metals by De-alloying Multicomponent Metallic Glasses, *Chem. Mater*. 20 (2008) 4548–4550.

[16]. Y. Q. Zeng, S. Yang, H. Xiang, X. Dong, L. Chen, M. Chen, A. Inoue, X. Zhang, J. Jian, Multicomponent nanoporous metals prepared by de-alloying Pd80xNixP20 metallic glasses. *Intermetallics* 61 (2015) 66-71.

[17]. X. Y. Lang, H. Guo, L. Y. Chen, A. Kudo, J. S. Yu, W. Zhang, M. W. Chen, A. Inoue, Novel Nanoporous Au-Pd Alloy with High Catalytic Activity and Excellent Stability. *J. Phys. Chem*. C 114 (2010) 2600–2603.

[18]. F. Scaglione, P. Rizzi, L. Battezzati, De-alloying kinetics of an Au-based amorphous alloy. *J. Alloys and Compd.* 536S (2012) S60-S64.

[19]. P. Rizzi, F. Scaglione, L. Battezzati, Nanoporous gold by dealloying of an amorphous precursor, *J. Alloys and Compd.* 586 (2014) S117–S120.

[20]. E. M. Paschalidou, F. Scaglione, A. Gebert, S. Oswald, P. Rizzi, L. Battezzati, Partially and fully de-alloyed glassy ribbons based on Au: application in methanol electro-oxidation studies, *J. Alloys and Compd.* 667 (2016) 302-309.

[21]. H. Guo, W. Zhang, C. Qin, J. Qiang, M. Chen, A. Inoue, Glass-Forming Ability and Properties of New Au-Based Glassy Alloys with Low Au Concentrations, *Mater. Trans*. 50 (2009) 1290- 1293.

[22]. K. F. Kelton, A. L. Greer, *Nucleation in Condenced Matter - Applications in Materials and Biology*, Pergamon Materials Series 15 , Press Elsevier, 2010.

[23] W. Liu , S. Zhang , N. Li , J. Zheng , S. An, G. Li, Influence of Dealloying Solution on the Microstructure of Monolithic Nanoporous Copper through Chemical Dealloying of Al 30 at.% Cu Alloy *Int. J. Electrochem. Sci*., 7 (2012) 7993 - 8006

[24]. V. Kalai Vani, O. J. Kwon, S. M. Hong, E. Fleury, Synthesis of porous Cu from Al–Cu–Co decagonal quasicrystalline alloys *Philosophical Magazine* 91 (2011) 2920-2928

[25] J. Xia, S. Ambrozik, C. C. Crane, J. Chen, N. Dimitrov, Impact of Structure and Composition on the Dealloying of $Cu_x$ $Au_{(1-x)}$ -Bulk and Nanoscale Alloys J. Phys. Chem. C 120 (2016) 2299-2308

[26] I. McCue, E. Benn, B. Gaskey, J. Erlebacher, Dealloying and Dealloyed Materials MR46CH01- Annu. Rev. Mater. Res. 2016

[27]. S. H. Lee, J. A. Stephens, G. S. Hwang, On the Nature and Origin of Si Surface Segregation in Amorphous Au-Si Alloys. *J. Phys. Chem.* C 114 (2010) 3037–3041.

[28]. H. Fujii, S. Tahara, Y. Kato, S. Kohara, M. Itou, Y. Kawakita, S. Takeda, Structural properties of liquid Au-Si and Au-Ge alloys with deep eutectic region, *J. of Non-Cryst.* Solids 353 (2007) 2094–2098.

[29]. E. S. Tasci, M. H. F. Sluiter, A. Pasturel, P. Villars, Liquid structure as a guide for phase stability in the solid state: Discovery of a stable compound in the Au–Si alloy system. *Acta Mater.* 58 (2010) 449–456.

[30]. D. Li, at al. Direction-Specific Interactions Control Crystal Growth by Oriented Attachment. *Science* 336 (2012) 1014-1018.

[31]. S. Parida, D. Kramer, C. A. Volkert, H. Rösner, J. Erlebacher, J. Weissmüller, Volume Change during the Formation of Nanoporous Gold by Dealloying, *Phys. Rev. Lett.* 97 (2006) 035504.

[32]. G. Gupta, J. C. Thorp, N. A. Mara, A. M. Dattelbaum, A. Misra, S. T. Picraux, Morphology and porosity of nanoporous Au thin films formed by dealloying of $Au_xSi_{(1-x)}$ . *J. of Appl. Phys.* 112 (2012) 094320.

[33]. P. G. Shewmon, *Diffusion in Solids*, Press McGraw-Hill, New York, 1963. Chapter 6.

[34]. M. Zhang, M.P. Li, T. Yin. T. Zhang, Fabrication of nanoporous bi-metallic Ag–Pd alloys with open pores, *Mat. Lett.* 162 (2016) 273-276.

[35]. F. Scaglione, E. M. Paschalidou, P. Rizzi, S. Bordiga, L. Battezzati, Nanoporous gold obtained from a metallic glass precursor used as substrate for surface-enhanced Raman scattering *Phil. Mag. Lett.* 95 (2015) 474–482.

[36]. E. D. Hondros, M. P. Seah, Segregation to interfaces, *Internet. Metall*. Rev. 22, (1977) 261-301.

**Figure 1**

Fig.1: Polarization curves of the amorphous $Au_{40}Cu_{28}Ag_7Pd_5Si_{20}$ (black), and the crystalline $Au_{31}Cu_{41}Mn_{15.2}Zn_{12.8}$(blue), and $Au_{37.5}Cu_{47.5}Ag_{6.25}Pd_{8.75}$ (red) alloys in 1M $HNO_3$ at 70°C.

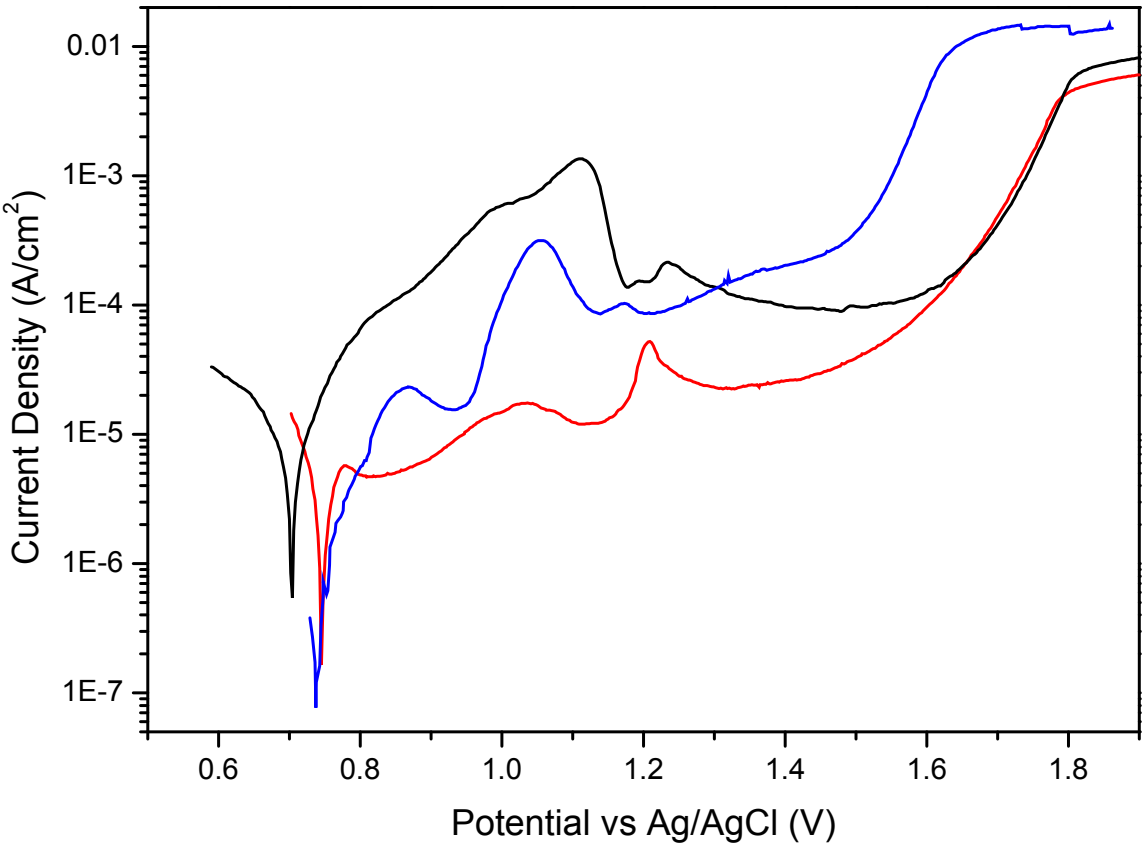

**Figure 2**

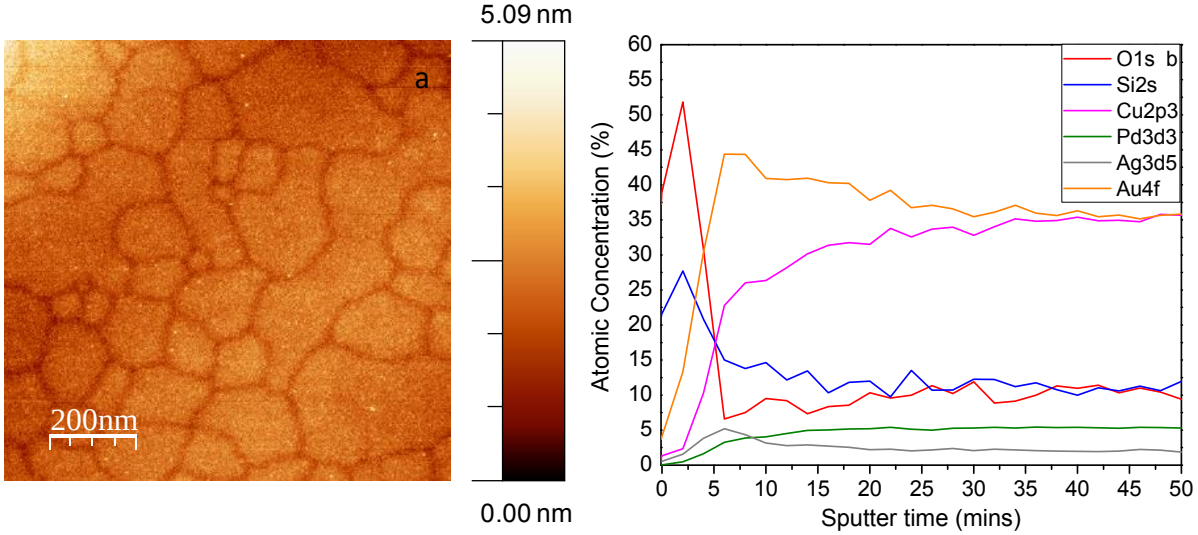
a
200nm
5.09 nm
0.00 nm
Atomic Concentration (%)
Sputter time (mins)
O1s b
Si2s
Cu2p3
Pd3d3
Ag3d5
Au4f
0
5
10
15
20
25
30
35
40
45
50
55
60

Figure 3

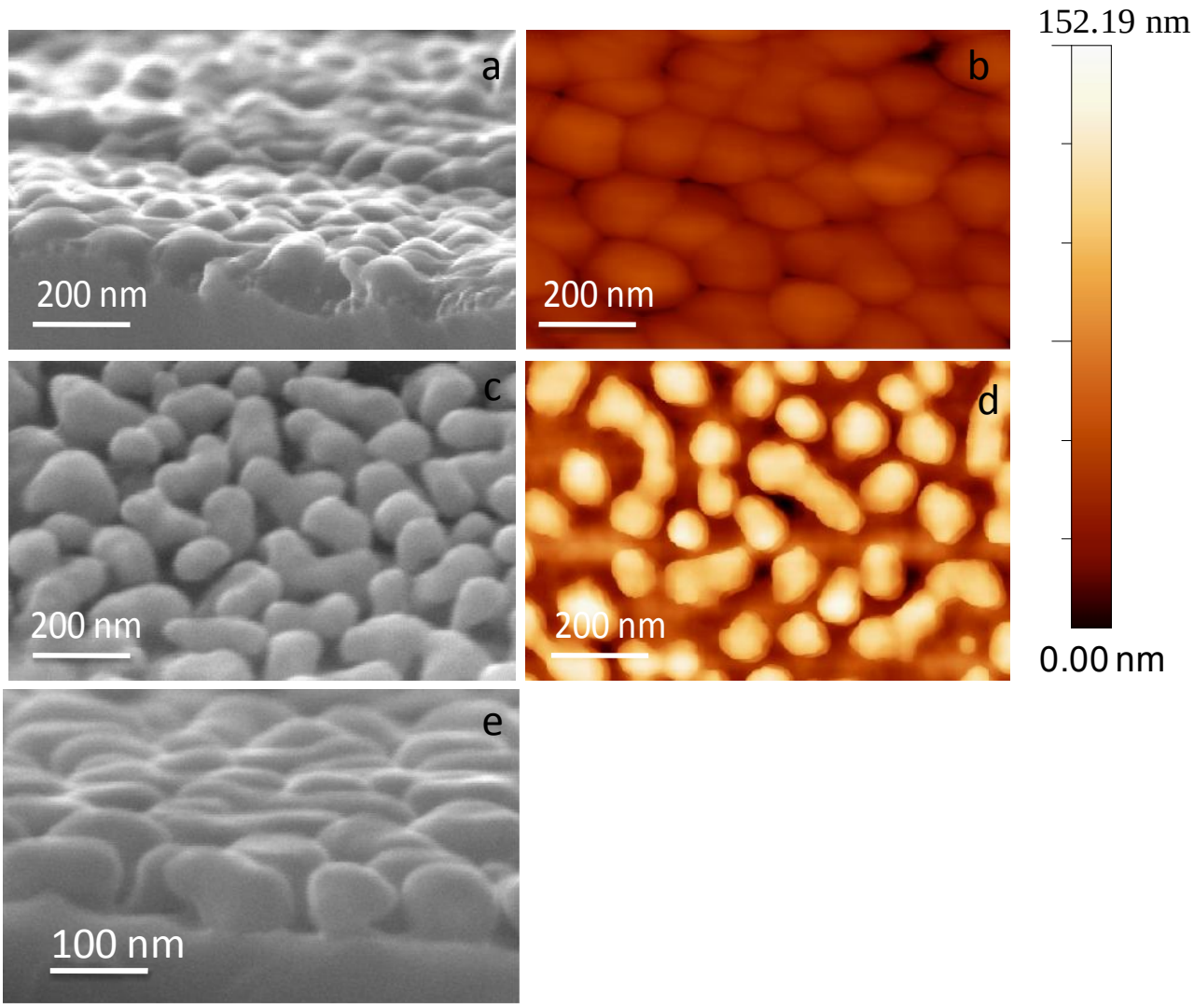

**Figure 4**

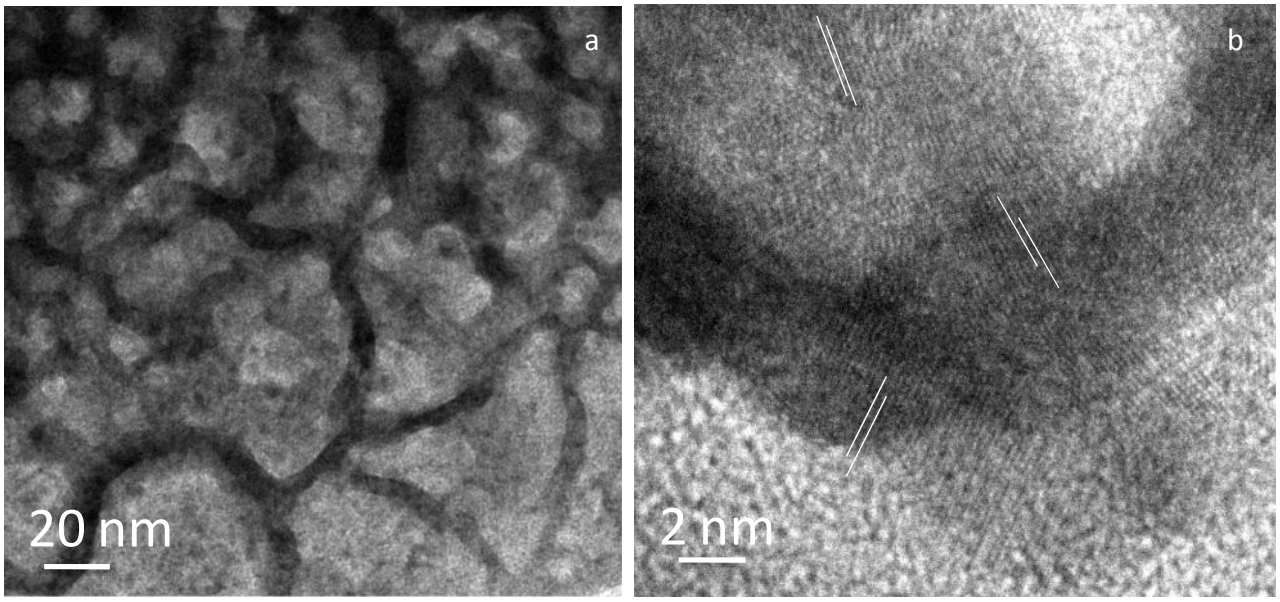

**Figure 5**

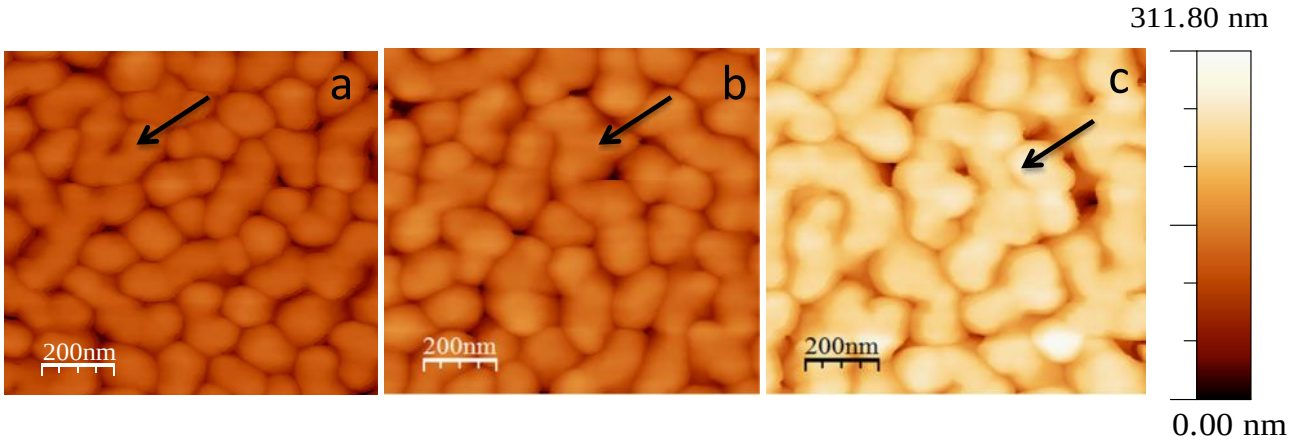

Figure 6

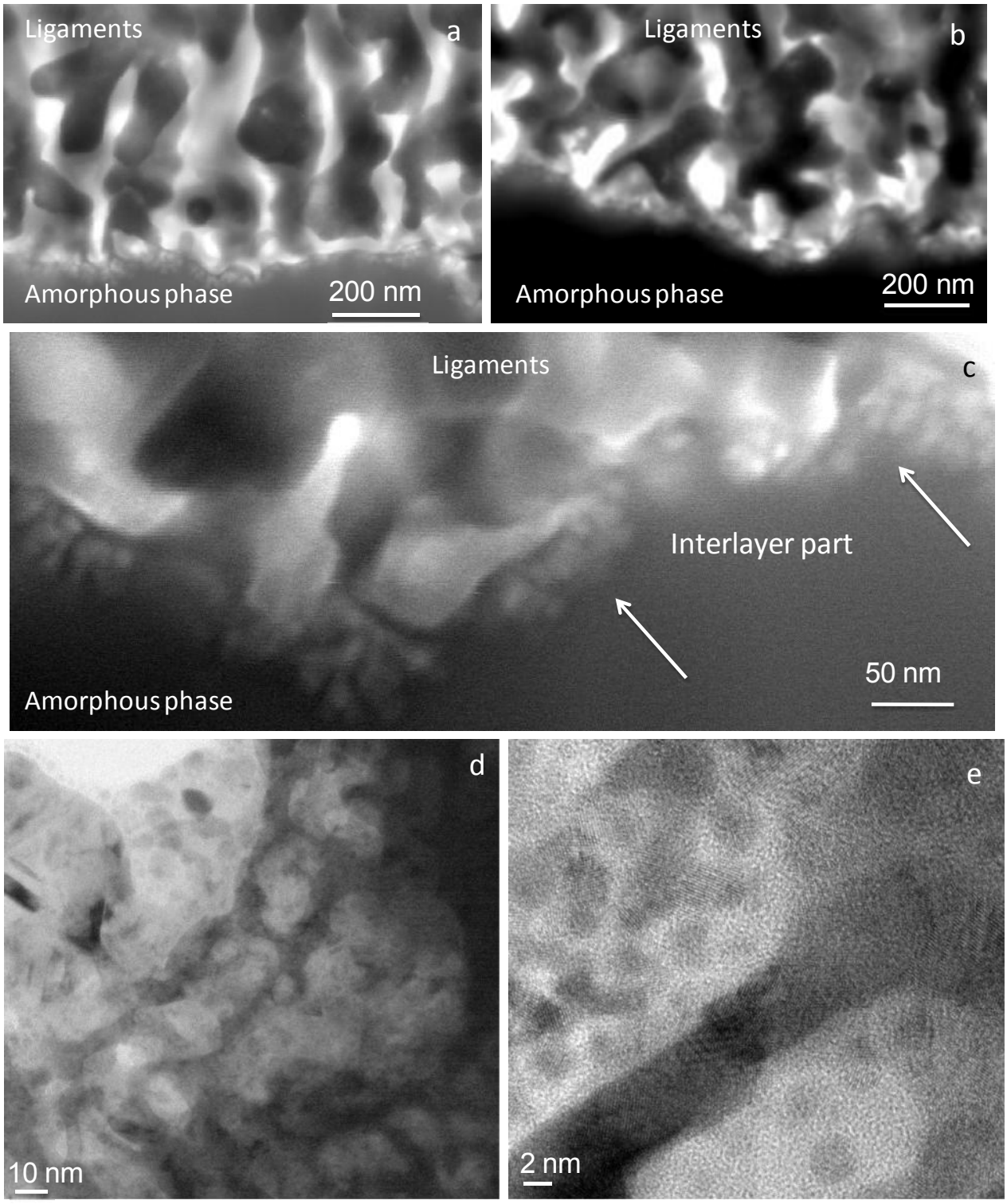
Ligaments
a
Amorphous phase
200 nm
Ligaments
b
Amorphous phase
200 nm
Ligaments
c
Interlayer part
Amorphous phase
50 nm
d
10 nm
e
2 nm